J. Fluid Mech. (1999), *vol.* 391, *pp.* 67–89. Printed in the United Kingdom

On the collision rate of small particles in turbulent flows

By RENWEI MEI AND KEVIN C. HU

Department of Aerospace Engineering, Mechanics and Engineering Science,
University of Florida, Gainesville, FL 32611-6250, USA
e-mail: rwm@aero.ufl.edu

(Received 5 March 1998 and in revised form 8 February 1999)

A theoretical framework is developed to predict the rate of geometric collision and the collision velocity of small size inertialess particles in general turbulent flows. The present approach evaluates the collision rate for small size, inertialess particles in a given instantaneous flow field based on the local eigenvalues of the rate-of-strain tensor. An ensemble average is then applied to the instantaneous collision rate to obtain the average collision rate. The collision rates predicted by Smoluchowski (1917) for laminar shear flow and by Saffman & Turner (1956) for isotropic turbulence are recovered. The collision velocities presently predicted in both laminar shear flow and isotropic turbulence agree well with the results from numerical simulations for particle collision in both flows. The present theory for evaluating the collision rate and the collision velocity is also applied to a rapidly sheared homogeneous turbulence to assess the effect of strong anisotropy on the collision rate. Using $(\varepsilon/\nu)^{1/2}$, in which ε is the average turbulence energy dissipation rate and ν is the fluid kinematic viscosity, as the characteristic turbulence shear rate to normalize the collision rate, the effect of the turbulence structure on the collision rate and collision velocity can be reliably described. The combined effects of the mean flow shear and the turbulence shear on the collision rate and collision velocity are elucidated.

1. Introduction

The rate of flow-induced particle collisions affects directly the particle size distribution in a particle production system. Examples of turbulence-induced particle collision can be seen in the formation of rain drops in clouds, pulverized coal combustion, agglomeration of fine powders in gas flows, air filtration equipment, sewage disposal devices, fast fluidized beds, dust and spray burners, and so on. Population balance equations are often used for predicting the evolution of particle size distribution in particle production systems or in studying particle coagulation. They are typically

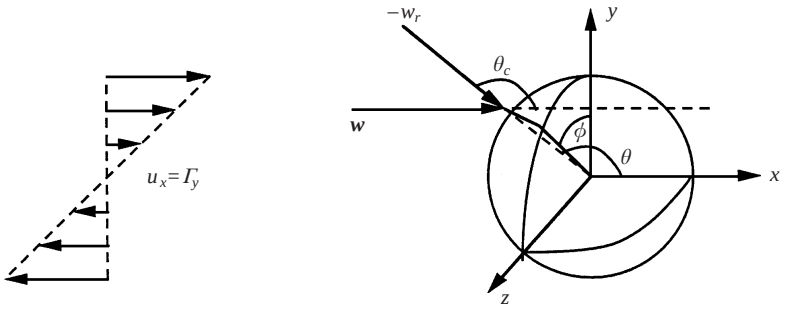

FIGURE 1. Local coordinates for collision in laminar shear flow.

given in the form of

$$\left.\begin{aligned}
\frac{\mathrm{d}n_1}{\mathrm{d}t} &= -\alpha_{11}n_1n_1 - \alpha_{12}n_1n_2 - \alpha_{13}n_1n_3 - \cdots \\
\frac{\mathrm{d}n_2}{\mathrm{d}t} &= \tfrac{1}{2}\alpha_{11}n_1n_1 - \alpha_{12}n_1n_2 - \alpha_{22}n_2n_2 - \alpha_{23}n_2n_3 - \cdots \\
\frac{\mathrm{d}n_3}{\mathrm{d}t} &= \alpha_{12}n_1n_2 - \alpha_{13}n_1n_3 - \alpha_{23}n_2n_3 - \alpha_{33}n_3n_3 - \cdots \\
\frac{\mathrm{d}n_4}{\mathrm{d}t} &= \alpha_{13}n_1n_3 + \tfrac{1}{2}\alpha_{22}n_2n_2 - \alpha_{14}n_1n_4 - \alpha_{24}n_2n_4 - \cdots \\
&\vdots
\end{aligned}\right\} \tag{1}$$

In the above, n_i is the number concentration of the ith particle size group. For primary particles, $i = 1$, with a volume v_1, the particle in the ith group has a volume of iv_1. The quantity $\alpha_{ij}n_in_j$, denoted as $\dot{N}_{ij}$ in this paper, is called the collision rate. It represents the number of collisions among the ith particle size group with the jth particle size group per unit volume and per unit time. The coefficient α_{ij} is called the collision kernel or collision function and must be evaluated separately. The determination of α_{ij} in a general turbulent flow for small particles with very small inertia is the primary focus of this paper. In reality, particle collision and the particle size-evolution are not only controlled by the fluid flow and particle inertia but also affected by the local particle–fluid and particle–particle interactions. A turbulent shear may bring two particles to collide; such an event is called a geometric collision. Whether these two particles stick to form a new particle or repel from each other depends on the local fluid–particle and the particle–particle interaction forces. When these two particles stick, a coagulation event has occurred. The probability for the colliding particles to coagulate can be taken into account in equation (1) by multiplying the collision function with a factor called collision efficiency. To determine the rate of geometric collision, it is a reasonable first step to neglect the particle–fluid and particle–particle interactions. It must also be pointed out that when equation (1) is used to predict the particle size evolution, it is necessary for particles in the system to be genuinely mixed.

Smoluchowski (1917) considered the collision rate among spherical particles in a laminar shear flow, $(u_x, u_y, u_z) = (\Gamma y, 0, 0)$ with a constant gradient $\partial u_x/\partial y = \Gamma$. For a target particle of radius r_i centred at an arbitrary position $\boldsymbol{x}_i$, any particle with a radius r_j moving toward the target particle will cause a geometric collision if

$$|\boldsymbol{x}_i - \boldsymbol{x}_j| \leqslant R_{ij} = r_i + r_j$$

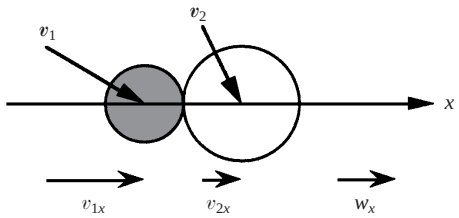

FIGURE 2. Sketch of particle collision velocity. The separation distance is $x_2 - x_1 = \pm R_{ij} = \pm(r_i + r_j)$.

is satisfied. The rate of the geometric collision can be evaluated as

$$\dot{N}_{ij} = n_i n_j \int_{w_r<0} -w_r \mathrm{d}A, \tag{2}$$

where w_r is the radial component of the relative fluid velocity between $\boldsymbol{x}_i$ and $\boldsymbol{x}_j$, $w_r < 0$ indicates an impending collision, $-n_1 n_2 w_r$ is the particle flux moving inward to the target particle, and A is the spherical surface with radius $R_{ij} = r_i + r_j$. Using standard spherical coordinates (R, θ, ϕ) centred at the target particle (see figure 1), w_r on the spherical surface of radius R_{ij} can be written as $w_r = \Gamma y \cos\theta = R_{ij} \sin\theta \cos\theta \cos\phi$. With $\mathrm{d}A = R_{ij}^2 \sin\theta \, \mathrm{d}\theta \, \mathrm{d}\phi$, it is easily seen that

$$\dot{N}_{ij} = n_i n_j \tfrac{4}{3} \Gamma R_{ij}^3 \tag{3}$$

or

$$\alpha_{ij} = \tfrac{4}{3} \Gamma R_{ij}^3. \tag{4}$$

Saffman & Turner (1956, hereinafter referred as ST) presented a classical theory for the rate of geometric collision among small particles in a Gaussian, isotropic turbulence. The collision rate among particle size group i and group j is

$$\dot{N}_{ij} = n_i n_j \left\langle \int_{w_r<0} -w_r \mathrm{d}A \right\rangle. \tag{5}$$

The ensemble average, denoted by $\langle\ \rangle$, is necessary since $-w_r$ due to turbulence is random. Because of the continuity of the fluid flow, the volume influx entering the spherical surface of radius R_{ij} is equal to the efflux which results in

$$\dot{N}_{ij} = \tfrac{1}{2} n_i n_j \left\langle \int_{\text{entire sphere}} |w_r| \mathrm{d}A \right\rangle. \tag{6}$$

ST further interchanged the integration with the ensemble average so that $\dot{N}_{ij}$ can be evaluated in an isotropic turbulence,

$$\dot{N}_{ij} \approx \tfrac{1}{2} n_i n_j \int_{\text{entire sphere}} \langle |w_r| \rangle \, \mathrm{d}A. \tag{7}$$

For an isotropic turbulence, the above becomes

$$\dot{N}_{ij} = n_i n_j 2\pi R_{ij}^2 \langle |w_x| \rangle, \tag{8}$$

where x is the local coordinate parallel to the line connecting the centres of the colliding particles, as shown in figure 2. For particle size smaller than the Kolmogorov

lengthscale η, the relative velocity upon the collision was evaluated using the standard results of small-scale turbulence theory,

$$\langle |w_x| \rangle = \langle |u_{ix} - u_{jx}| \rangle \approx R_{ij} \left\langle \left| \frac{\partial u}{\partial x} \right| \right\rangle = R_{ij} \left(\frac{2}{15\pi} \frac{\varepsilon}{\nu} \right)^{1/2} \tag{9}$$

where ε is the energy dissipation rate of the turbulence and ν is fluid kinematic viscosity. This gives

$$\dot{N}_{ij} = n_i n_j R_{ij}^3 \left(\frac{8}{15\pi} \frac{\varepsilon}{\nu} \right)^{1/2} = 1.2944 n_i n_j R_{ij}^3 \left(\frac{\varepsilon}{\nu} \right)^{1/2}, \tag{10}$$

or

$$\alpha_{ij} = 1.2944 R_{ij}^3 \left(\frac{\varepsilon}{\nu} \right)^{1/2}, \tag{11}$$

or

$$\alpha_{ij}^* = \frac{\alpha_{ij}}{R_{ij}^3 (\varepsilon/\nu)^{1/2}} = 1.2944, \tag{12}$$

where α_{ij}^* is the normalized collision coefficient or collision kernel.

Balachandar (1988) performed numerical simulations to examine the validity of the ST theory. He found a significant effect of the preferential concentration on the increase of the collision rate as the particle inertia increases. However, the ST theory in the zero-inertia, small-size limit cannot be validated for two reasons. (i) The probability distribution of $\partial u/\partial x$ was found to be log-normal, instead of Gaussian as assumed in ST's theory, in the direct numerical simulation (DNS) of turbulence. This results in a correction to ST's prediction for the collision rate. (ii) Particle size much larger than the Kolmogorov lengthscale η was used in his simulation while ST's theory is for particles with size $r_i \ll \eta$. Chen, Kontomaris & Mclaughlin (1995) studied the particle collision and deposition in a two-dimensional turbulent channel flow using the turbulence field generated by DNS. They found a significant non-uniformity in the concentration distribution because the particulate flow is inherently inhomogeneous. Recently, Wang, Wexler & Zhou (1998) examined ST's theory by using DNS results for the turbulence to evaluate the particle collision rate in an isotropic turbulence. Their results indicate that the collision rate depends on the implementation of the post-collision treatment. For a certain implementation, the collision rate can be smaller than that given by ST by as much as 15% for particles with finite size but zero inertia.

It must be pointed out that from equation (6) to equation (7), the interchange between the integration with the ensemble average is only an approximation even in a Gaussian, isotropic turbulence. Furthermore, the interchange between these two operations severely limits the extension of ST's result and approach to other turbulent flows such as the near-wall region where the mean flow gradient contributes to $\langle |w_r| \rangle$. Of course, in the theory of Smoluchowski for laminar shear flow, this issue does not arise since the ensemble average over velocity is not needed so that there is no difference between equations (6) and (7). However, in the numerical simulation to determine the particle collision rate in a laminar shear flow, the ensemble average over the initial particle positions can be used to improve the statistics. In a typical industrial facility where particle collision leads to the desirable growth of particles, the inhomogeneity of the turbulent flow structure is common. Owing to the effects such as turbulence inhomogeneity, particles tend to be driven toward the near-wall region to cause a further inhomogeneity in the particle concentration distribution. It

was not clear how the collision rate of small particles in the presence of both strong mean flow shear and high turbulence intensity could be predicted (K. Kontamaris 1995, private communication).

In this paper, a theoretical framework is presented for evaluating the rate of the geometric collision of inertialess particles, whose sizes are smaller than the Kolmogorov lengthscale, in general turbulent flows. The present analysis starts from equation (5). Using the leading-order term, $(\boldsymbol{x}_i - \boldsymbol{x}_j)\cdot\nabla\boldsymbol{u}$, in the Taylor series expansion to approximate the relative fluid velocity, $\boldsymbol{w}$, at the collision instant, the collision rate for an arbitrarily given $\nabla\boldsymbol{u}$ is evaluated first. The ensemble average is subsequently performed to obtain the local particle collision rate for a given flow. This theory is applied to a Gaussian, isotropic turbulence to obtain the collision rate and collision velocity in an isotropic turbulence. Numerical simulations based on Lagrangian particle tracking are also performed to obtain the collision rate and collision velocity directly in the Gaussian, isotropic turbulence. Good agreement is obtained between the present prediction and the numerical simulation for the collision kernel α_{ij}^*. Excellent agreement is obtained for the average collision velocity between the prediction and the simulation. While the present result for the collision rate agrees with the prediction of ST, the present theory predicts an average collision velocity at the instant of collision, $\langle -w_r | w_{r<0} \rangle$, that is 1.58 times the value given by ST. The difference is caused by the bias of the collision toward regions of higher collision velocity which was not considered in previous studies on flow-induced particle collisions. Since whether the colliding particles coagulate or not depends, to a large extent, on the magnitude of the relative velocity of the colliding particles (to overcome the attractive surface forces), it is important that $\langle -w_r | w_{r<0} \rangle$ and $\langle w_r^2 | w_{r<0} \rangle$ be predicted correctly. Using the rapid distortion theory (RDT) for a rapidly sheared homogeneous turbulence and the random Fourier modes representation of turbulence, the dependence of particle collision kernel α_{ij} on the mean flow shear rate and the turbulence structure in the homogeneous turbulent shear flow is studied under the present theoretical framework. The effect of the turbulence structure on the collision rate and collision velocity can be captured by using a characteristic turbulent shear rate $(\varepsilon/\nu)^{1/2}$ in which ε is the energy dissipation rate of turbulence under rapid shear. The collision kernel, after normalization by particle volume and $(\varepsilon/\nu)^{1/2}$, mainly depends on the ratio of the mean flow shear rate to $(\varepsilon/\nu)^{1/2}$.

2. Analysis

The relative fluid velocity between the target particle centred at $\boldsymbol{x}_1$ and the colliding particle centred at $\boldsymbol{x}_2$ is $\boldsymbol{w} = \boldsymbol{u}_1 - \boldsymbol{u}_2$ and the relative position between $\boldsymbol{x}_1$ and $\boldsymbol{x}_2$ is

$$\boldsymbol{r}_{12} = \boldsymbol{x}_2 - \boldsymbol{x}_1. \tag{13}$$

For $R = |\boldsymbol{r}_{12}| < \eta$, the relative velocity $\boldsymbol{w}$ can be expressed using the Taylor series expansion as

$$\boldsymbol{w} = \boldsymbol{u}_2 - \boldsymbol{u}_1 \approx \boldsymbol{r}_{12}\cdot\nabla\boldsymbol{u} + \cdots \quad \text{for } |\boldsymbol{r}_{12}| < \eta, \tag{14}$$

to the leading order. The collision rate for a given $\nabla\boldsymbol{u}$ at the spatial location $\boldsymbol{x} = \boldsymbol{x}_1$ at a given instant is

$$\dot{N}_{12}(t, \boldsymbol{x}) = n_1 n_2 \int_{w_r<0} -\boldsymbol{w}\cdot\boldsymbol{n}\,\mathrm{d}A, \tag{15}$$

where $\boldsymbol{n}$ is the outward normal of the surface given by $|\boldsymbol{x}_2 - \boldsymbol{x}_1| = R$ and $w_r = \boldsymbol{w} \cdot \boldsymbol{n}$. On the spherical surface $|\boldsymbol{r}_{12}| = R$, it is obvious that $\boldsymbol{n} = \boldsymbol{r}_{12}/R$. Hence,

$$\int_{w_r<0} -\boldsymbol{w} \cdot \boldsymbol{n} \mathrm{d}A = \frac{1}{R} \int_{w_r<0} -\boldsymbol{w} \cdot \boldsymbol{r}_{12} \mathrm{d}A \approx \frac{1}{R} \int_{w_r<0} -\boldsymbol{r}_{12} \cdot \nabla \boldsymbol{u} \cdot \boldsymbol{r}_{12} \mathrm{d}A. \tag{16}$$

Representing $\nabla \boldsymbol{u}$ as the sum of a symmetrical part (rate-of-strain tensor) and an anti-symmetrical part (vorticity tensor), it can be easily seen that the anti-symmetrical part of $\nabla \boldsymbol{u}$ does not contribute to w_r. Physically, it is simply because a rigid-body rotation does not contribute to the normal velocity. For a symmetric tensor $\boldsymbol{E} = \frac{1}{2}(\nabla \boldsymbol{u} + (\nabla \boldsymbol{u})^T)$, or a symmetric matrix E_{ij}, a linear transformation, which is a rotation of the coordinate system from (x, y, z) to $(\hat{x}, \hat{y}, \hat{z})$, can be easily found to reduce E_{ij} to a diagonal form as

$$\hat{\boldsymbol{E}} = \begin{bmatrix} e_{\hat{x}} & 0 & 0 \\ 0 & e_{\hat{y}} & 0 \\ 0 & 0 & e_{\hat{z}} \end{bmatrix}, \tag{17}$$

where $(e_{\hat{x}}, e_{\hat{y}}, e_{\hat{z}})$ are the eigenvalues of $\boldsymbol{E}$ and they are the principal values of the rate-of-strain tensor. Because of the incompressibility, $e_{\hat{x}} + e_{\hat{y}} + e_{\hat{z}} = 0$ so that there are only two independent parameters (say $e_{\hat{x}}$ and $e_{\hat{y}}$) in $\hat{\boldsymbol{E}}$. For the purpose of evaluating the integral in equation (16), the eigenvalues $(e_{\hat{x}}, e_{\hat{y}}, e_{\hat{z}})$ may be arranged in ascending order as

$$e_{\hat{z}} = -(e_{\hat{x}} + e_{\hat{y}}) \leqslant e_{\hat{y}} \leqslant e_{\hat{x}}. \tag{18}$$

Defining

$$\zeta = \frac{e_{\hat{y}}}{e_{\hat{x}}} \quad \text{with} \quad -0.5 \leqslant \zeta \leqslant 1, \tag{19}$$

the integrand in equation (16) can be expressed as

$$\begin{aligned} -\boldsymbol{r}_{12} \cdot \nabla \boldsymbol{u} \cdot \boldsymbol{r}_{12} &= -(e_{\hat{x}} \hat{x}^2 + e_{\hat{y}} \hat{y}^2 + e_{\hat{z}} \hat{z}^2) = -e_{\hat{x}}[\hat{x}^2 + \zeta \hat{y}^2 - (1 + \zeta)\hat{z}^2] \\ &= -e_{\hat{x}} R^2 [\cos^2 \theta + \zeta \sin^2 \theta \cos^2 \phi - (1 + \zeta) \sin^2 \theta \sin^2 \phi], \end{aligned} \tag{20}$$

where a local spherical coordinate system ($\hat{x} = R \cos\theta$, $\hat{y} = R \sin\theta \cos\phi$, $\hat{z} = R \sin\theta \sin\phi$) has been employed. Hence,

$$\begin{aligned} &\int_{w_r<0} -\boldsymbol{w} \cdot \boldsymbol{n} \, \mathrm{d}A \\ &\quad = -R^3 e_{\hat{x}} \int_0^{2\pi} \int_{0\ w_r<0}^{\pi} [\cos^2 \theta + \zeta \sin^2 \theta \cos^2 \phi - (1 + \zeta) \sin^2 \theta \sin^2 \phi] \sin\theta \, \mathrm{d}\theta \, \mathrm{d}\phi \\ &\quad = R^3 e_{\hat{x}} H(\zeta). \end{aligned} \tag{21}$$

Again, $w_r < 0$ in the integration limit implies that only the non-positive values inside the square brackets are evaluated in the integration. Whereas an analytical expression for $H(\zeta)$ is difficult to obtain owing to the dependence of the integration limits on arbitrary ζ, accurate numerical integration for $H(\zeta)$ can be carried out in a straightforward manner (using Simpson's rule in this work). The following interpolation is then constructed for $H(\zeta)$ based on the results of numerical integration,

$$\begin{aligned} H(\zeta) &\approx \tfrac{8}{3}[0.90725 + 0.2875(0.5 + \zeta)^2 + 0.33333(0.5 + \zeta)^4] \qquad (\zeta < 0) \\ &\approx \tfrac{8}{3}[1 + 0.55\zeta + 0.72407\zeta^2 - 0.96874\zeta^3 + 0.73924\zeta^4 - 0.23035\zeta^5] \quad (\zeta \geqslant 0). \end{aligned} \tag{22}$$

The above piecewise polynomial fitting differs from the results of numerical integration by less than 0.1%. Consider the laminar shear flow, for example. In this case, $\zeta = 0$, $e_{\hat{x}} = \frac{1}{2}\Gamma, H(0) = \frac{8}{3}$, so that $\dot{N}_{12} = n_1 n_2 \frac{1}{2}\Gamma R^3 \frac{8}{3} = n_1 n_2 \frac{4}{3}\Gamma R^3$ which is the same as given by Smoluchowski (1917).

Equation (22) is valid for $-1 \leqslant \zeta \leqslant -0.5$ as well, since it is based on (21). The restriction for $\zeta \geqslant -0.5$ given by (19) results only from (18) when the eigenvalues are arranged in such a manner. For $-1 \leqslant \zeta \leqslant -0.5$, $H(\zeta)$ is symmetric with respect to $\zeta = -0.5$ and this fact has been used in constructing the curve fitting given by (22) for $\zeta < 0$. For example, $\zeta = 0$ corresponds to a two-dimensional stagnation flow in the $(\hat{x}, \hat{z})$-plane, and $\zeta = -1$ corresponds to a two-dimensional stagnation flow in the $(\hat{x}, \hat{y})$-plane, so that the collision rates for $\zeta = 0$ and $\zeta = -1$ are completely equivalent. It is also interesting to note that $\zeta = -0.5$ is equivalent to $\zeta = 1$ since both correspond to an axisymmetric stagnation flow. For $\zeta = -0.5$, the local flow experiences an axisymmetric contraction with the $\hat{x}$-axis being the axis of symmetry. For $\zeta = 1$, the local flow is an axisymmetric expansion with the $\hat{z}$-axis being the axis of the symmetry and flow decelerates along the $\hat{z}$-direction. The only difference is the scale factor $e_{\hat{x}}$. The direction of the flow or the sign of $e_{\hat{x}}$ does not affect the collision rate since the integration only picks up the contribution from the part of the colliding surface where $w_r = \boldsymbol{w} \cdot \boldsymbol{n} < 0$. For $\zeta \geqslant 0$, it is seen that,

$$(e_{\hat{x}}, e_{\hat{y}}, e_{\hat{z}}) = e_{\hat{x}}(1, \zeta, -(1+\zeta)) = e_{\hat{z}} \left(-\frac{1}{1+\zeta}, -\frac{\zeta}{1+\zeta}, 1 \right),$$

where $|e_{\hat{z}}| = |e_{\hat{x}}|(1+\zeta)$. Hence,

$$H(0 \leqslant \zeta \leqslant 1) = (1+\zeta) H\left(-\frac{1}{1+\zeta} \right).$$

Similarly,

$$H\left(-\frac{1}{1+\zeta} \right) = H\left(-\frac{\zeta}{1+\zeta} \right)$$

since $H(\zeta)$ is symmetric with respect to $\zeta = -0.5$ for $\zeta \leqslant 0$. Thus, $H(\zeta \leqslant 0)$ can be obtained from $H(\zeta \geqslant 0)$ as

$$H\left(-\frac{1}{1+\zeta} \right) = H\left(\frac{1}{1+\zeta} - 1 \right) = \frac{1}{1+\zeta} H(\zeta) \quad \text{for } \zeta \geqslant 0. \tag{23}$$

Finally, the collision rate for small size, inertialess particles in a turbulent flow is simply obtained by taking the ensemble average over all possible values of the rate-of-strain tensor as

$$\dot{N}_{12}(\boldsymbol{x}, t) = n_1 n_2 R^3 \langle e_{\hat{x}} H(\zeta) \rangle . \tag{24}$$

It is emphasized that this result is applicable to general turbulent flows since $n_i, e_{\hat{x}}$, and ζ are all functions of $\boldsymbol{x}$ and t. Needless to say, the isotropy assumption is eliminated in this framework. When the detailed knowledge of $\nabla \boldsymbol{u}$ is available, such as from DNS or random Fourier modes representation (Kraichnan 1970) of turbulence, the ensemble average in (24) can be carried out. The local, ensemble-averaged collision rate is thus obtained.

The foregoing analysis can also be extended to evaluate the average of the normal (or radial) component of the collision velocity $\langle -w_r|_{w_r<0} \rangle$. It is noted that the average collision velocity is always a conditional average under the condition $w_r < 0$. Hereinafter, the notation $w_r < 0$ is dropped for simplicity with the understanding that

$\langle -w_r \rangle = \langle -w_r|_{w_r<0} \rangle$, and $\langle w_r^2 \rangle = \langle w_r^2|_{w_r<0} \rangle$. At a given location $\boldsymbol{x}$ with arbitrary $e_{\hat{x}}$ and ζ at any given instant, the instantaneous average of the normal collision velocity can be calculated by integrating over the spherical surface of radius R as

$$\langle w_r|e_{\hat{x}}, \zeta \rangle^{\mathscr{A}} = \frac{\int_{w_r<0} w_r(-w_r)\mathrm{d}A}{\int_{w_r<0}(-w_r)\mathrm{d}A}. \tag{25}$$

In the above, the superscript $\mathscr{A}$ on the left-hand side denotes the area-average on the colliding surface of radius $R = r_1 + r_2$, $(-w_r)\mathrm{d}A$ in the numerator can be interpreted as proportional to the probability of a particle striking the colliding surface at a position (θ, ϕ) over an area $\mathrm{d}A$ and w_r in the numerator is the relative radial velocity of the collision at (θ, ϕ) on the colliding surface. The denominator is the normalizing factor for the probability. The product, $w_r(-w_r)$, clearly indicates that $\langle w_r|e_{\hat{x}}, \zeta \rangle^{\mathscr{A}}$ is a biased average in favour of those regions on the colliding surface where $(-w_r)$ is high. Suppose that N_R realizations of turbulence be taken in a turbulent flow. Based on (5), the total number of collision per unit time will be

$$N_c = N_R n_1 n_2 \left\langle \int_{w_r<0} (-w_r)\mathrm{d}A \right\rangle.$$

The chance of a particle striking the target surface over an area $\mathrm{d}A$ at (θ, ϕ) relative to the axis of the principal direction $\hat{x}$ in a given realization is then $n_1 n_2(-w_r)\mathrm{d}A|_{w_r<0} N_c$. Integrating over the target surface of radius R and summing over N_R realizations, the ensemble averaged $\langle w_r \rangle$ is obtained,

$$\langle w_r \rangle = N_R \left\langle \int_{w_r<0} w_r \frac{n_1 n_2(-w_r)}{N_c}\mathrm{d}A \right\rangle = \frac{\left\langle \int_{w_r<0} w_r(-w_r)\mathrm{d}A \right\rangle}{\left\langle \int_{w_r<0}(-w_r)\mathrm{d}A \right\rangle}. \tag{26}$$

The above can be simplified to

$$\langle w_r \rangle = -R \left\langle e_{\hat{x}}^2 G(\zeta) \right\rangle / \langle e_{\hat{x}} H(\zeta) \rangle, \tag{27}$$

where

$$G(\zeta) = \int_0^{2\pi} \int_{0\ w_r<0}^{\pi} [\cos^2\theta + \zeta\ \sin^2\theta\ \cos^2\phi - (1+\zeta)\ \sin^2\theta\ \sin^2\phi]^2 \sin\theta\ \mathrm{d}\theta\, \mathrm{d}\phi. \tag{28}$$

The integration can again be evaluated numerically and represented in the following piecewise polynomials

$$\begin{aligned} G(\zeta)/H(\zeta) &= 0.4 + 1.0777(0.5+\zeta)^2 - 0.64767(0.5+\zeta)^4 \quad \text{for } \zeta < 0 \\ &= 0.62831 + 0.68495\zeta - 0.091083\zeta^2 \\ &\quad + 0.090301\zeta^3 - 0.034658\zeta^4 \qquad \text{for } \zeta \geqslant 0. \end{aligned} \tag{29}$$

Similarly, the mean square value of the radial component of the collision velocity $\langle w_r^2 \rangle$ can be evaluated as

$$\langle w_r^2 \rangle = R^2 \left\langle e_{\hat{x}}^3 K(\zeta) \right\rangle / \langle e_{\hat{x}} H(\zeta) \rangle, \tag{30}$$

with

$$\begin{aligned} K(\zeta)/H(\zeta) &= 0.17114 + 1.2643(0.5+\zeta)^2 - 0.48123(0.5+\zeta)^4 \quad \text{for } \zeta < 0 \\ &= 0.45714 + 0.97655\zeta + 0.39606\zeta^2 \\ &\quad + 0.072430\zeta^3 - 0.0291\zeta^4 \qquad \text{for } \zeta \geqslant 0. \end{aligned} \tag{31}$$

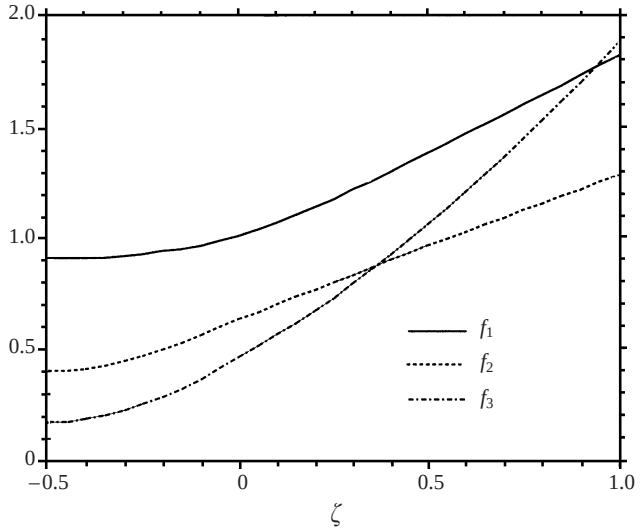

FIGURE 3. Variations of $H(\zeta), G(\zeta), K(\zeta)$ with ζ where $f_1 = \frac{3}{8}H(\zeta), f_2 = G(\zeta)/H(\zeta)$ and $f_3 = K(\zeta)/H(\zeta)$.

The functions $H(\zeta), G(\zeta)/H(\zeta)$, and $K(\zeta)/H(\zeta)$ are shown in figure 3. Take a laminar shear flow for example: $e_{\hat{x}} = \frac{1}{2}\Gamma$ and $\zeta = 0$ so that $G/H = 0.62832(= \frac{1}{5}\pi)$ and $K/H = \frac{16}{35}$. It is easily seen that

$$\langle w_r \rangle = -R\tfrac{1}{4}\Gamma^2\tfrac{1}{5}\pi\tfrac{8}{3}/[\tfrac{1}{2}\Gamma\tfrac{8}{3}] = -\tfrac{1}{10}\pi\Gamma R, \tag{32}$$

$$\langle w_r^2 \rangle = R^2\tfrac{1}{8}\Gamma^3\tfrac{16}{35}\tfrac{8}{3}/[\tfrac{1}{2}\Gamma\tfrac{8}{3}] = \tfrac{4}{35}(\Gamma R)^2. \tag{33}$$

These results can be used to validate the present theoretical formulation by comparing them with the numerical simulation results of particle collision based on Lagrangian tracking.

To apply the above results to turbulent flows, we consider the following two cases: (i) a Gaussian isotropic turbulence; and (ii) a rapidly sheared homogeneous turbulence under a mean flow gradient $\partial u_x/\partial y = \Gamma$. In both cases, the turbulence can be represented using random Fourier modes and ensemble averages can be obtained without resorting to the direct numerical solutions to the Navier–Stokes equations for the fluid flows. Pertinent comparison can be made with ST's prediction in the first case. Insights on the effects of mean flow shear can be gained by examining the collision rate in the rapidly sheared turbulence.

The detailed representation of the isotropic turbulence and rapidly sheared homogeneous turbulence are given in the Appendix. In short, the isotropic turbulence is expressed as in equation (A 6). For sheared homogeneous turbulence, the flow field is given by equation (A 18).

3. Numerical simulation of particle collision in isotropic turbulence

3.1. *Random Fourier modes representation of fluid turbulence in a periodic box*

The velocity field of the Gaussian isotropic turbulence is first generated by a random Fourier modes representation (A 6). To effectively conduct a computational study on particle collision, a finite region should be used and periodic boundary conditions are enforced to ensure the continuity in the velocity field. We choose a box of volume π^3.

To render the turbulence represented by random Fourier modes periodic in this box, the random wavenumbers, $k_i^{(m)}$, are rounded to the nearest even integers while all other quantities are held fixed so that the flow is periodic within the box of volume π^3. The periodic box of volume π^3 yields virtually the same collision statistics when the volume is increased to $(2\pi)^3$. Hence, π^3 is used throughout this study for efficient numerical simulation of particle collisions. The corresponding statistics, such as turbulence root-mean-squared (r.m.s.) velocity u_0, Reynolds number Re_λ, Taylor micro lengthscale λ, Kolmogorov lengthscale η, and Kolmogorov timescale τ_k, are computed based on the modified wavenumbers. Using the present analysis outlined in § 2, the collision statistics, when normalized using $(\varepsilon/\nu)^{1/2}$ for α_{11} and $\langle -w_r \rangle$, remain the same whether we use the turbulence generated for an unbounded domain or for a periodic box.

A number of particles (N_p) are randomly introduced in the flow field of volume π^3. Their motions are advanced using $u_i(\boldsymbol{x}, t)$ given by (A 6) with a timestep Δt. Their trajectories are computed with a second-order scheme.

3.2. *Collision detection scheme*

Collision detection between any particle pair (Balachandar 1988; Chen *et al.* 1995) is briefly described as follows. At the nth timestep t_n, two particles are located at $\boldsymbol{x}_1(t_n)$ and $\boldsymbol{x}_2(t_n)$, respectively. At time $t_{n+1} = t_n + \Delta t$, they are advanced to $\boldsymbol{x}_1(t_{n+1})$ and $\boldsymbol{x}_2(t_{n+1})$. The distance between two particles can be expressed as

$$\mathrm{d}(t) = |\boldsymbol{x}_2(t) - \boldsymbol{x}_1(t)| \quad \text{for } t_n \leqslant t \leqslant t_{n+1}. \tag{34}$$

The pair collide during this period of time if $\mathrm{d}(t) \leqslant R_{ij}$.

In general, the collision detection requires searching the collision pairs among all N_p particles; this takes $O(N^2)$ operations. In this study, the collision detection method described by Balachandar (1988) and Chen *et al.* (1995) is implemented. By dividing the computational domain of volume π^3 into a number of smaller cells, the potential collision partners for a given particle in one cell are then searched within this cell and its twenty-six neighbouring cells during one timestep. This search involves a much smaller number of particles than in the entire domain. Only binary collision is considered by assuming a negligible probability of multiple collisions within a small timestep in the dilute condition. Any particle that moves out of the computational box is reintroduced into the box by invoking the periodicity. The collision rate or coefficient can be determined, in principle, by counting the number of collisions per timestep.

3.3. *Post-collision treatment*

A collision is counted when two particles are brought into contact. How the colliding particles are treated after the collision may have a significant effect on future particle collision. In the work by Chen *et al.* (1995) a 'keep all' scheme was used. Every collision results in the colliding particles disappearing from their respective size groups and a larger particle being generated. Both mass and momentum conservation laws were applied for the birth of this new particle. Balachandar (1988) used a different post-collision scheme. Starting with monosize particles in the system, the resulting larger particle was discarded from the flow field after each collision so that it would not contribute to future collisions. This post-collision treatment is hereinafter referred as a 'throw away' scheme. Sundaram & Collins (1996) employed a hard sphere collision model. Particles were forced to bounce back after each collision. Wang *et al.* (1998) tested three different schemes; two of them allow the colliding particles to overlap in space (hereinafter referred as an 'overlapping' scheme) but no larger particles are formed after the collision. These two colliding particles can separate after their tra-

Particle radius	$\langle -w_r \rangle$ simulation	$\langle -w_r \rangle$ prediction	$\langle w_r^2 \rangle$ simulation	$\langle w_r^2 \rangle$ prediction
0.009	5.6421×10^{-3}	5.6549×10^{-3}	3.7018×10^{-5}	3.7029×10^{-5}
0.0125	7.8638×10^{-3}	7.8540×10^{-3}	7.1529×10^{-5}	7.1429×10^{-5}
0.02	1.2425×10^{-2}	1.2566×10^{-3}	1.8012×10^{-4}	1.8286×10^{-4}

TABLE 1. Comparison of the collision velocity among monosized particles between prediction and direct numerical simulation in laminar shear flow.

jectories satisfy $\mathrm{d}(t) \leqslant R_{ij}$. Thus, a particle of a given size can have multiple collisions within a short period of time. These four different post-collision treatments will, in principle, result in different collision rates and it is not clear which treatment is the best.

In this work, the 'throw away' scheme is implemented. However, an extremely low particle volume concentration is used. The initial particle volume concentration is chosen carefully so that the average number of collisions in each turbulence realization is less than 1. The post-collision treatment thus has little practical effect on the collision statistics. A large number of turbulence realizations are used to obtain reliable ensemble average. A subsequent cumulative time averaging smoothes out statistical noise in the collision rate.

4. Results and discussions

4.1. *Comparison with simulation results in a laminar shear flow*

In an earlier paper dealing with particle collision a laminar shear flow (Hu & Mei 1998), comparison for the collision kernel, $\frac{4}{3}\Gamma R^3$, based on Smoluchowski's prediction and the numerical simulation was presented; excellent agreement was obtained. To confirm the present analyses in the laminar shear flow, we compare the collision velocity given by (32) and (33) with that based on the numerical simulations. Inertialess particles of radius 0.009, 0.0125 and 0.02, respectively, are introduced into a cubic box with length $L_x = 2.0$, $L_y = 2.0$, and $L_z = 2.0$, with the restriction of $0.1 < y_p < 1.9$ in which y_p is the y-coordinate of the particle position. A uniform shear flow with a shear rate $\Gamma = 1.0$ is imposed and the flow velocity field is given by $\boldsymbol{v} = (u_x, u_y, u_z) = (\Gamma y, 0, 0)$. Periodic boundary conditions are employed in the streamwise and spanwise directions. Particles near $y = 0.1$ and $y = 1.9$ have fewer collisions because there are no particles in regions of $y < 0.1$ and $y > 1.9$ in the simulation. A correction due to this boundary effect (Wang *et al.* 1998) was needed for the collision rate (Hu & Mei 1998). However, this boundary correction has little effect on the collision velocity since the decrease in the collision frequency affects both the numerator and denominator in (25). Three hundred timesteps with a step size $\Delta t = 0.01$ are used to advance particles and a total of 40 realizations are employed to further increase the statistical accuracy. Ten thousand particles are used for $r = 0.009, 0.0125$, while four thousand particles are used for larger size with $r = 0.02$. Table 1 shows the comparisons for both $\langle -w_r \rangle$ and $\langle w_r^2 \rangle$. Since $\langle w_r^2 \rangle$ is the second-order moment of w_r, excellent agreement for these two moments indicates that the basis of the present formulation is sound. It is worth noting that a naive, Eulerian-based estimation of the average collision velocity based on the incoming particle flux, $\frac{4}{3}\Gamma R^3 n_i$, and the available collision area, $2\pi R^2$, would lead to an erroneous value of $\frac{2}{3}(1/\pi)\Gamma R$ instead of $\frac{1}{10}\pi\Gamma R$ for $\langle -w_r \rangle$.

In a laminar shear flow, $w_r = -u_x \cos\theta$ and the collision angle θ_c between the

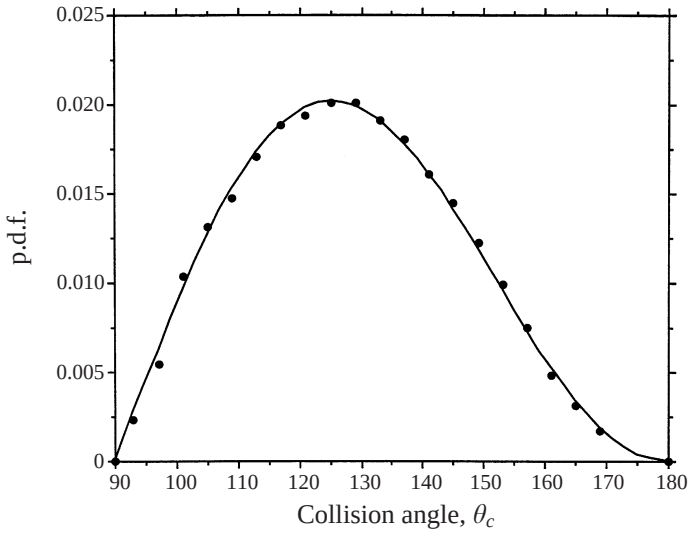

FIGURE 4. Comparison of the p.d.f.s for the collision angles θ_c between —, the theory and •, the simulation in laminar shear flow.

collision velocity $\boldsymbol{w}$ and the axis connecting the centres of the colliding particle pair, $\frac{1}{2}\pi \leqslant \theta_c \leqslant \pi$, happens to be equal to θ, as shown in figure 1. In the simulation, θ_c can be evaluated easily so that the probability density function (p.d.f.) for θ_c is readily obtained. Since $(-w_r)_{w_r<0} \sin\theta d\,\theta d\phi$ is proportional to the probability of the particle striking the target surface at (θ, ϕ) with a solid angle $\mathrm{d}\omega = \mathrm{d}\theta\,\mathrm{d}\phi$, it is readily seen that

$$\begin{aligned}(-w_r)\mathrm{d}A &= -\Gamma R^3 \sin^2\theta \cos\theta \cos\phi\, \mathrm{d}\theta\mathrm{d}\phi \quad \text{for } (\theta,\phi) \in \Omega \\ &= 0 \qquad\qquad\qquad\qquad\qquad\quad \text{elsewhere,}\end{aligned} \tag{35}$$

where Ω is the region defined by ($\frac{1}{2}\pi \leqslant \theta \leqslant \pi$, $-\frac{1}{2}\pi \leqslant \phi \leqslant \frac{1}{2}\pi$) and ($0 \leqslant \theta \leqslant \frac{1}{2}\pi$, $\frac{1}{2}\pi \leqslant \phi \leqslant \frac{3}{2}\pi$) in which $w_r \leqslant 0$. Interpreting $\sin^2\theta\cos\theta\sin\phi$ as proportional to the p.d.f. of incoming particles striking the target particle near (θ, ϕ), further integrating over ϕ from 0 to 2π, treating $0 \leqslant \theta \leqslant \frac{1}{2}\pi$ as the same as $\frac{1}{2}\pi \leqslant \theta \leqslant \pi$ due to the symmetry, and using appropriate normalization, one obtains the p.d.f. for the collision angle θ_c

$$\begin{aligned}p(\theta_c) &= -B \sin^2\theta_c \cos\theta_c \quad \text{for } \pi \leqslant \theta \leqslant \tfrac{1}{2}\pi \\ &= 0 \qquad\qquad\qquad\quad \text{for } 0 \leqslant \theta \leqslant \tfrac{1}{2}\pi,\end{aligned} \tag{36}$$

where B is a normalizing factor which is 3 for θ_c in radians and $\frac{1}{60}\pi$ for θ_c in degrees. The average angle is $\langle\theta_c\rangle = \int_{1/2\pi}^{\pi} \theta_c\, p(\theta_c)\mathrm{d}\theta_c = 2.237$ rad or 128.17°. The numerical simulation gives $\langle\theta_c\rangle = 128.13^\circ$. Figure 4 compares the p.d.f.s based on the above prediction and the numerical simulation using ten thousand particles of radius 0.009 over 40 realizations of initial particle positions. Excellent agreement is observed for the whole region $\frac{1}{2}\pi \leqslant \theta_c \leqslant \pi$. The present theoretical framework is thus validated in the laminar shear flow.

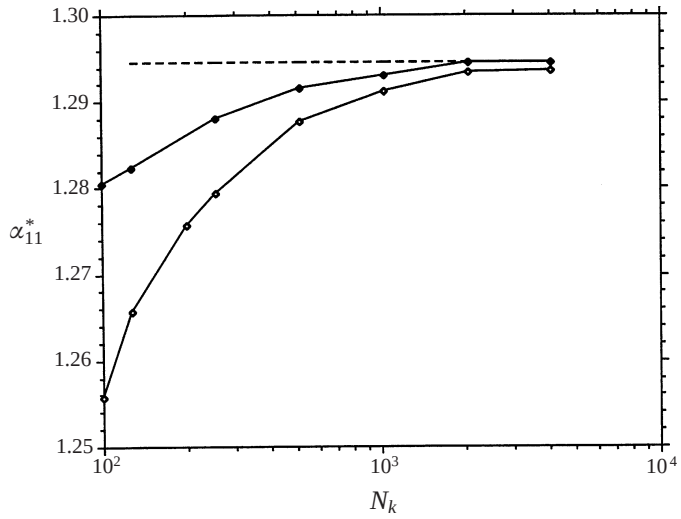

FIGURE 5. Convergence of α_{11}^* as $N_k \to \infty$. - - -, Saffman & Turner (1956); ◆, $\mu = 1.4$; ◇, $\mu = 1.2$.

4.2. *Collision rate and collision velocity in a Gaussian, isotropic turbulence*

For particle collision in isotropic turbulence which is represented using (A 6), the dimensionless collision kernel,

$$\alpha_{11}^* = \frac{\alpha_{11}}{R^3(\varepsilon/\nu)^{1/2}} = \frac{\langle e_{\hat{x}} H(\zeta)\rangle}{(\varepsilon/\nu)^{1/2}}, \tag{37}$$

is evaluated using $N_R = 500$ realizations. The dissipation rate ε is based on the ensemble average of the same N_R realizations. In each realization, $e_{\hat{x}} H(\zeta)$ and ε/ν are computed in the flow field with about 654 statistically independent data. It is found that α_{11}^* varies slightly with the number of Fourier modes, N_k, used in the turbulence representation. Furthermore, it weakly depends on the power μ in (A 10) with which the random wavenumbers are chosen. Figure 5 shows the variation of α_{11}^* as N_k increases from 100 to 4096 for $\mu = 1.2$ and 1.4 for $\bar{\eta}_0 = 0.05$ ($Re_\lambda = 53.8$). The result seems to converge after $N_k = 2048$; $\alpha_{11}^*(\mu = 1.2)$ converges to 1.2935 while $\alpha_{11}^*(\mu = 1.4)$ converges to 1.2945 with a difference of less than 0.1%. They are both very close to 1.2944, the value predicted by ST. It is worth commenting that owing to the rapid decrease of the energy spectrum $E(k)$ in the high k range, not all wavenumbers that are randomly generated need to be used in (A 10). Those high-wavenumber modes corresponding to very small amplitudes can be neglected without compromising the accuracy. Thus, the effective number of random modes is smaller than the specified N_k. From the simulations, the effective number of the modes for $\mu = 1.4$ is roughly three times of that for $\mu = 1.2$ for the same N_k. Hence, the fact that it takes larger values of N_k for $\mu = 1.2$ than for $\mu = 1.4$ to obtain a converged result is not surprising. It is also interesting to note that, using $N_k = 1024$ and $\mu = 1.2$, a higher values of Re_λ(= 124.4 using $\bar{\eta}_0 = 0.01$) gives $\alpha_{11}^* = 1.2899$ as opposed to $\alpha_{11}^* = 1.2912$ at $Re_\lambda = 53.8$. This clearly shows that shape of the energy spectrum $E(k)$ or the value of Re_λ in isotropic turbulence has little effect on α_{11}^*. With $N_k = 200$ and $\mu = 1.2$, $\alpha_{11}^* = 1.2756$ which is only 1.45% less than the converged result. Thus, in the following numerical simulation for counting the number of particle collisions, $N_k = 200$ and $\mu = 1.2$ is used.

Particle radius (r/η)	$\langle -w_r \rangle$ simulation	$\langle -w_r \rangle$ prediction	$\langle w_r^2 \rangle$ simulation	$\langle w_r^2 \rangle$ prediction
0.217	4.5430×10^{-2}	4.4931×10^{-2}	2.7356×10^{-3}	2.7296×10^{-3}
0.4875	1.0093×10^{-1}	1.0076×10^{-1}	1.3405×10^{-2}	1.3224×10^{-2}

TABLE 2. Comparison of the collision velocity among monosized particles between prediction and direct numerical simulation in a Gaussian, isotropic turbulence.

To validate the present analyses, numerical simulations of particle collision in isotropic turbulence are performed. The turbulence in the periodic box of length π has the following characteristics: r.m.s. turbulence velocity $u_0 = 1.0$, integral lengthscale $L_{11} = 0.594$, Taylor micro lengthscale $\lambda = 0.277$, Kolmogorov lengthscale $\eta = 0.023$, Kolmogorov timescale $\tau_k = (\nu/\varepsilon)^{1/2} = 0.073$, and $Re_\lambda = 40.1$. With the modified Fourier modes in the periodic box, the dimensionless collision kernel based on the prediction is $\alpha_{11}^* = 1.2711$ as opposed to $\alpha_{11}^* = 1.2756$ (see the above paragraph) without the modification of the wavenumbers. Initially, five hundred particles of radius $r = 0.005$ ($r/\eta = 0.217$) are randomly distributed in the box of volume π^3 with a particle volume concentration of 8.44×10^{-6}. These inertialess particles are advanced using local fluid velocity. A total time period of $T = 6$ (i.e. $T/\tau_k = 82.2$) is simulated with timestep $\Delta t = 0.01$. The average number of collisions within the entire period of the simulation $0 < t < T = 6$ in each realization is about $0.4271 < 1$. To obtain reliable statistics, a total of 10 000 realizations is used to generate an estimated number of collision pairs $N_C = 4271$. Figure 6(a) shows the simulation result for α_{11}^* in $0 < t/\tau_k < 82.2$ and the predicted value of 1.2711. There is a significant noise in the numerical simulation data due to the small number of collisions within each timestep despite the fact that 10 000 realizations have been used. A cumulative average is applied to reduce the noise. Figure 6(b) shows the cumulative time average of α_{11}^* from the simulation. The result of the numerical simulation is less than the predicted value (1.2711) by about 2.5%. This difference may be caused by the particle size effect, since the theoretical predictions are expected to be accurate only in the small size limit, $r/\eta \ll 1$, while the particle size in the numerical simulation is $r/\eta = 0.217$. The effect of finite particle size on the collision rate will be explored separately. The agreement for α_{11}^* between the simulation and the prediction is quite good.

Table 2 shows the results of the prediction and the numerical simulation for the two moments of particle collision velocity, $\langle -w_r \rangle$ and $\langle w_r^2 \rangle$, in isotropic turbulence. The predicted values are based on $\mu = 1.2$ and $N_k = 200$ in the periodic box with $N_R = 400$ realizations. The particle sizes are $r/\eta = 0.2175$ and 0.4875, respectively. Satisfactory agreements are obtained. On the other hand, ST gave an expression, equation (9), for the Eulerian-based average particle radial collision velocity. Using that expression would give $\langle -w_r \rangle / R(\varepsilon/\nu)^{1/2} = 0.206$. The present prediction for the turbulence in the periodic domain with $N_R = 400$, after ensemble average, gives a value of 0.328 for this dimensionless radial collision velocity which agrees rather well with the numerical simulation shown in table 2. Since the numerical simulation is based on the tracking of particle trajectories, the probability-based prediction for $\langle -w_r \rangle$ is consistent with the Lagrangian approach. The Eulerian-based approach for $\langle -w_r \rangle$ does not take into account the bias of the collision probability toward the high values of $-w_r$; hence, it gives a lower value for $\langle -w_r \rangle$.

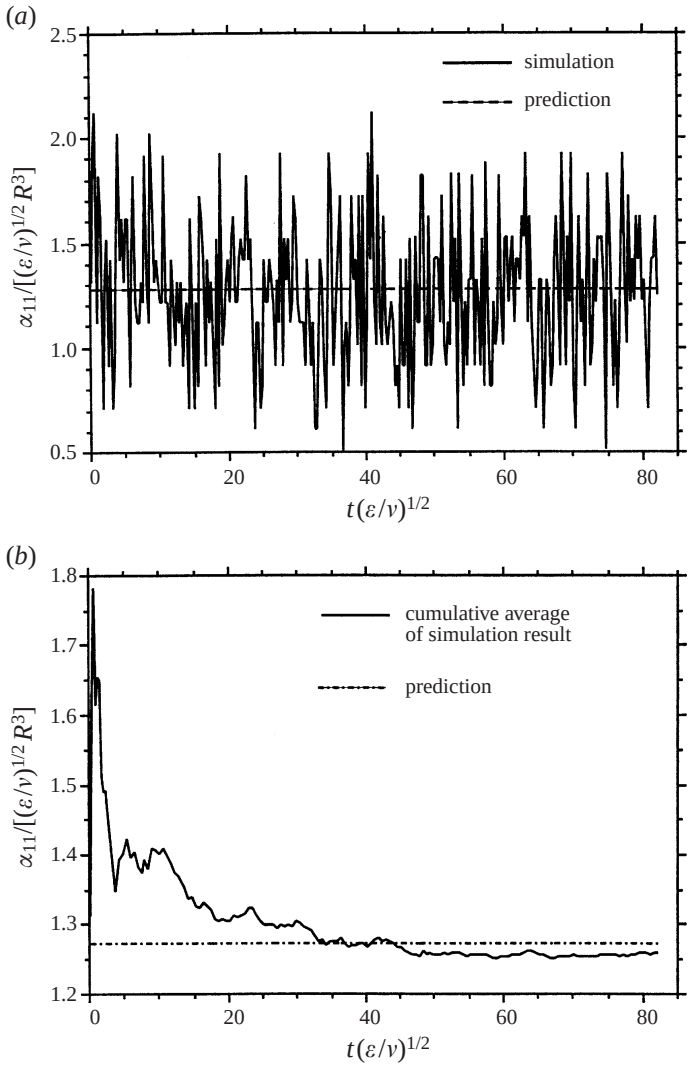

FIGURE 6. (*a*) Variation of the ensemble averaged particle collision kernel α_{11}^* from direct numerical simulation in isotropic turbulence. (*b*) Cumulative time average of α_{11}^*.

4.3. *Collision in a rapidly sheared homogeneous turbulence*

The statistics of the turbulence, such as four non-zero components of the Reynolds stress tensor, generated using RDT and the random Fourier modes were first checked against the analytical values at short times ($\Gamma t \ll 1$) given by RDT (Townsend 1976, p. 84) and the numerical results of Lee, Kim & Moin (1990) for a finite period of time to ensure the correct implementations. Interested readers can find relevant information on the structure of rapidly sheared turbulence in the works by Townsend (1976) and Lee *et al.* (1990). It was found through simulation that the development of the sheared turbulence with time does not depend on the Reynolds number, Re_λ, of the initial state or the energy spectrum at $t = 0$. The turbulence part of the flow in the RDT is determined by the total shear $S = \Gamma t$. The complete flow field, sheared turbulence plus the mean shear flow, thus depend on two parameters: Γ and $S = \Gamma t$. Since the

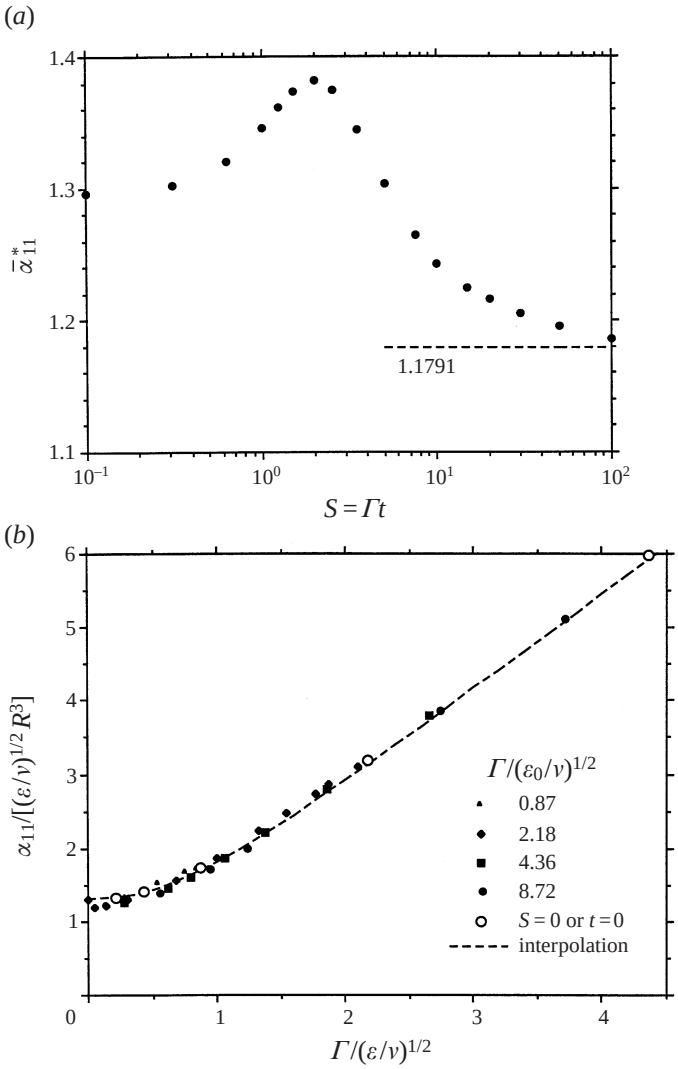

FIGURE 7. (*a*) Normalized particle collision rate in highly sheared homogeneous turbulence without contribution from the mean shear rate. (*b*) Collision rate in a rapidly sheared homogeneous turbulence. ε_0 denotes the dissipation rate of the isotropic state at $t = 0$.

collision rate depends on the spatial structure of the turbulence while the turbulence structure becomes increasingly anisotropic as the total shear S increases, finding an appropriate representation of the collision rate in the homogeneous turbulent shear flow is not trivial. In this part of the investigation, equations (22), (24), and (27)–(31) are used to compute the collision rate and collision velocity.

To develop a better understanding of the dependence of the collision rate on the turbulent flow, it is instructive to first examine the collision rate due to the sheared turbulence alone without the contribution from the mean shear Γ; this part of the collision kernel will be denoted as $\bar{\alpha}_{11}$. Another word, $\bar{\alpha}_{11}$ is evaluated using the flow field given by (A 18) but without the last deterministic term $\Gamma x_2 \delta_{i1}$. Following the definition for α^*_{11} in the isotropic turbulence case, we use $(\varepsilon/\nu)^{1/2}$, which increases

rapidly with S, as the turbulence characteristic shear rate to normalize $\bar{\alpha}_{11}$,

$$\bar{\alpha}^*_{11} = \frac{\bar{\alpha}_{11}}{R^3(\varepsilon/\nu)^{1/2}} \quad \text{(without contribution from mean shear } \Gamma\text{)}. \tag{38}$$

It is easily seen that $\bar{\alpha}^*_{11}$ depends only on the total shear $S = \Gamma t$. Figure 7(a) shows the variation of $\bar{\alpha}^*_{11}$ on S. In the high S limit, the numerical results suggest that $\bar{\alpha}^*_{11}$ approach a constant of 1.1791 in the form of

$$\bar{\alpha}^*_{11} \sim 1.1791 + 0.8078/S \quad \text{for } S > 10. \tag{39}$$

In the range of $0 \leqslant S < 100$ turbulence goes from an isotropic state to a strongly anisotropic state. The turbulence intensity becomes dominated by the longitudinal component in the x_1-direction. Based on RDT prediction which neglects the nonlinear interaction among different scales, the longitudinal component of the turbulence makes up 92.7% of the total kinetic energy at $S = \Gamma t = 20$. The anisotropy invariant II_b reaches a value of -0.25 at $S = 20$. At such large values of total shear, S, the RDT results may become a little inaccurate in comparison with the result of the DNS of the Navier–Stokes equations. However, for the present work, since the RDT-based turbulence is strongly anisotropic, it serves our purpose to evaluate the effect of such anisotropy in the turbulence structure on the particle collision rate. When the collision kernel is normalized using $(\varepsilon/\nu)^{1/2}$, the maximum difference in $\bar{\alpha}^*_{11}$ is only about 15% at the extreme limit of $S \to \infty$. If the isotropic result is used, $\bar{\alpha}^*_{11} \sim 1.2944$, only a maximum error of 10% will result from the limiting value of $\bar{\alpha}^*_{11}$ at very large total shear. This encouraging result will be used to develop an approximation for $\bar{\alpha}^*_{11}$ in the presence of strong mean shear.

Now consideration is given to the particle collision kernel with contribution from both the turbulence part and the mean flow shear part as the flow field is given by the entire right-hand side of (A 18). Figure 7(b) shows α^*_{11} as a function of the ratio of the mean shear rate to the turbulence characteristic shear rate, $\Gamma/(\varepsilon/\nu)^{1/2}$, for a range of shear rates. For a given Γ, $(\varepsilon/\nu)^{1/2}$ increases as t or S increases so that the abscissa mainly reflects the effect of t or S. To see the effect of mean flow shear rate, Γ is made dimensionless by the initial isotropic state turbulence characteristic shear rate $(\varepsilon_0/\nu)^{1/2}$. Four values of $\Gamma/(\varepsilon_0/\nu)^{1/2}$ are used: 0.87, 2.18, 4.36, and 8.72; they correspond to the solid symbols in figure 7(b). The open symbols specifically correspond to the case when $S = 0$ (or $t = 0$) so that the turbulence is still isotropic. The dimensionless values of α^*_{11} seem to collapse reasonably well. At large values of $\Gamma/(\varepsilon/\nu)^{1/2}$, the curve becomes linear as the collision rate is increasingly dominated by the mean shear so that α_{11} scales linearly with Γ as Smoluchowski's theory predicts. A small degree of scattering exists for $\Gamma/(\varepsilon/\nu)^{1/2} < 2$. This is caused by the 15% maximum variation in $\bar{\alpha}^*_{11}$ over the whole range of S, as demonstrated in figure 7(a). There are two possibilities for $\Gamma/(\varepsilon/\nu)^{1/2} \ll 1$: (i) both Γ and $S = \Gamma t$ are very small, even comparing with $(\varepsilon_0/\nu)^{1/2}$ of the initial isotropic turbulence; (ii) Γ is finite but $S = \Gamma t$ is large so that $(\varepsilon/\nu)^{1/2}$ becomes large compared with $(\varepsilon_0/\nu)^{1/2}$. In the first case, the turbulence is closer to the isotropic state so that $\alpha^*_{11} \sim 1.2944$. In the second case, the turbulence is highly anisotropic and $\bar{\alpha}^*_{11} \to 1.1791$ for very large values of S. No attempt is made to correlate $\bar{\alpha}^*_{11}$ with the total shear S since S is not relevant in practical applications such as in turbulent pipe flow. Using $\alpha^*_{11} = 1.2944$ in the isotropic state to represent the turbulence part of the collision kernel, a simple interpolation is proposed to represent the effect of mean shear and turbulence on the

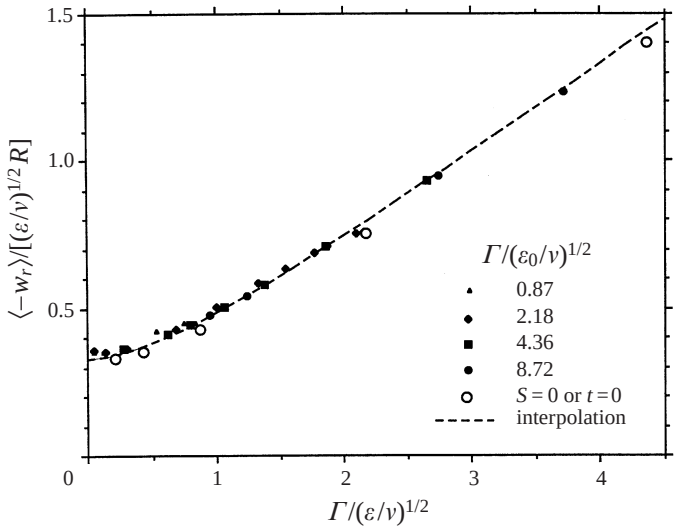

FIGURE 8. Collision velocity in a rapidly sheared homogeneous turbulence. ε_0 denotes the dissipation rate of the isotropic state at $t = 0$.

collision rate,

$$\alpha_{11}^* \approx \frac{\alpha_{11}}{R^3(\varepsilon/\nu)^{1/2}} = \left\{ 1.2944^{2.2} + \left[\frac{1.3333\Gamma}{(\varepsilon/\nu)^{1/2}} \right]^{2.2} \right\}^{1/2.2}. \tag{40}$$

This interpolation is represented by the dashed line in figure 7(*b*). A satisfactory agreement can be observed. It is also worth commenting that when Γ is normalized using the eddy turn over time, $3u_0^2/\varepsilon_0$, of the initial isotropic turbulence, the shear-rate parameter

$$\Gamma^* = \Gamma 3u_0^2/\varepsilon_0 \tag{41}$$

corresponds to $\Gamma^* = 36.98$ and 92.45 for $\Gamma/(\varepsilon_0/\nu)^{1/2} = 0.87$ and 2.18. In a low-Reynolds-number turbulent channel flow, the maximum value of Γ^* is around 35 at a location of 10 wall units away from the wall (Kim, Moin & Mosers 1987). Hence, the parameters used in figure 7(*b*) are relevant to practical situations. Although a 10% error exists for α_{11}^* given by (40), the advantage of this simple approximation is that the dependence on the total shear $S = \Gamma t$ is eliminated and α_{11}^* depends only on the scalar quantity $\Gamma(\nu/\varepsilon)^{1/2}$ that captures both the effects of spatial structure of the turbulence and the mean flow shear rate.

Figure 8 shows the radial collision velocity, $\langle -w_r \rangle$, as a function of $\Gamma/(\varepsilon/\nu)^{1/2}$, for different values of $\Gamma/(\varepsilon_0/\nu)^{1/2}$. Similarly, the data seem to collapse approximately into one curve in the range studied. The following interpolation fits the radial collision velocity well,

$$\frac{\langle -w_r \rangle}{R(\varepsilon/\nu)^{1/2}} \approx \left\{ 0.3245^{1.7} + \left[\frac{1}{10}\pi \frac{\Gamma}{(\varepsilon/\nu)^{1/2}} \right]^{1.7} \right\}^{1/1.7}. \tag{42}$$

For the r.m.s. radial collision velocity, $\langle w_r^2 \rangle$, the behaviour is very similar to that of $\langle -w_r \rangle$. While the data is not shown here for brevity, the following interpolation,

which fits the data quite well, is provided,

$$\frac{\langle w_r^2 \rangle^{1/2}}{R(\varepsilon/\nu)^{1/2}} = \left\{ 0.3681^{1.7} + \left[\frac{0.3381\Gamma}{(\varepsilon/\nu)^{1/2}} \right]^{1.7} \right\}^{1/1.7}. \tag{43}$$

The application of the above expressions to turbulent channel flow, which is different from the homogeneous, rapidly sheared turbulence, is yet to be tested. However, since the rapidly sheared turbulence at large total shear S considered in this work is already drastically different from the isotropic turbulence, there are reasons to expect a similar dependence of α_{11}, $\langle -w_r \rangle$, and $\langle w_r^2 \rangle$ on Γ and $(\varepsilon/\nu)^{1/2}$ in a turbulent channel flow which is of significant industrial importance.

Since the present theory is developed for particles with zero inertia, the effect of preferential concentration or the microscopic particle concentration non-uniformity cannot be included in this work. Additional efforts are required to include the effect of the particle inertia on the collision rate in the presence of mean shear.

5. Summary and conclusion

A theoretical framework has been developed to evaluate the collision rate and collision velocity of small particles in general turbulent flows. The present approach differs significantly from that of Saffman & Turner (1956) in that the ensemble average is taken after the collision rate for a given flow realization is calculated. This eliminates the assumption of isotropy, as needed in Saffman & Turner, and allows for the evaluation of the collision rate in general turbulent flows. Using the present theory, the classical results for the collision rate by Smoluchowski (1917) for laminar shear flow and by Saffman & Turner (1956) for isotropic turbulence are recovered. The predicted collision velocity in both laminar shear flow and isotropic turbulence agrees well with the numerical simulation result for particle collisions.

The present theory is subsequently used to evaluate the collision rate and collision velocity of small particles in the rapidly sheared homogeneous turbulence. Although the turbulence structure depends strongly on the total strain rate S and is highly anisotropic and the collision rate depends on the rate-of-strain tensor in general, it is found that the effect of the turbulence structure on the collision rate and collision velocity can be captured by using a characteristic turbulent shear rate $(\varepsilon/\nu)^{1/2}$. The combined effects of the mean shear and the sheared turbulence on the collision rate and the collision velocity can be reliably evaluated using simple interpolations for arbitrary mean flow shear rate and turbulence mean shear rate.

The authors acknowledge the financial support of the Engineering Research Center (ERC) for Particle Science and Technology at the University of Florida, the National Science Foundation (EEC-9402989), industrial partners of the ERC, and the ALCOA Foundation Award.

Appendix. Representation of isotropic turbulence and rapidly sheared turbulence

A.1. *Isotropic turbulence*

The following model for the energy spectrum developed in Mei & Adrian (1995) is assumed for turbulence,

$$E(k) = \tfrac{3}{2} u_0^2 \psi \frac{k^4}{k_0^5} \frac{1}{[1 + (k/k_0)^2]^{17/6}} \exp(-\eta_0^2 k^2), \tag{A 1}$$

where u_0 is the r.m.s. turbulent velocity, k_0 is a typical wavenumber and the dimensionless parameter $\bar{\eta}_0 = \eta_0 k_0$ is related to the turbulent Reynolds number Re_λ. Large Re_λ corresponds to small $\bar{\eta}_0$ and vice versa. The normalizing coefficient ψ in $E(k)$ is determined from (A 1) by satisfying the total energy requirement,

$$\psi^{-1} = \int_0^\infty \frac{\bar{k}^4}{(1+\bar{k}^2)^{17/6}} \exp(-\bar{\eta}_0^2 \bar{k}^2) \mathrm{d}\bar{k}. \tag{A 2}$$

For small $\bar{\eta}_0, E(k) \sim k^4$ when $\bar{k} = k/k_0 \ll 1$ and $E(k) \sim k^{-5/3}$, which is the scaling law in the inertial subrange, when $1 \ll \bar{k} \ll 1/\bar{\eta}_0$. For large $\bar{\eta}_0$, the above energy spectrum recovers that of Kraichnan (1970). The relationship between the Eulerian integral length $L_{11}k_0$ and $\bar{\eta}_0$, (or Re_λ) is given in Mei & Adrian (1994).

A turbulent eddy loses its identity as it is convected and dissipated; this behaviour is described by the eddy self-decay function $D(\tau)$ which has an integral timescale T_0. The Fourier transformation of $D(\tau)$ gives the power spectrum $\tilde{D}(\omega)$. A composite form for the power spectrum $\tilde{D}(\omega)$ was constructed in Mei & Adrian (1995) as

$$\tilde{D}(\omega) = \tilde{A} \frac{\exp(-\eta_1^2 \omega^2)}{1 + (T\omega)^2}, \tag{A 3}$$

where η_1 is intended for the viscous dissipation timescale if the turbulent Reynolds number is high, and T is close to T_0 if $\eta_1/T \ll 1$. The coefficient $\tilde{A}$ is determined as

$$\tilde{A} = \frac{T}{\pi} \frac{\exp(-\eta_1^2/T^2)}{1 - \mathrm{erf}(\eta_1/T)} \tag{A 4}$$

by satisfying $\int_{-\infty}^{\infty} \tilde{D}(\omega) \mathrm{d}\omega = 1$. The integral timescale T_0 is related to T as $T_0 = \pi \tilde{D}(0) = \pi \tilde{A}$.

The relationship between L_{11} and T_0 is not known in general; it can take the following form

$$T_0 = c^E(Re_\lambda) L_{11}/u_0, \tag{A 5}$$

where $c^E(Re_\lambda)$ was determined approximately in Mei & Adrian (1995) based on the experimental data of Sato & Yamamoto (1987) for the fluid dispersion and the value of high-Reynolds-number turbulent Prandtl number.

Using random Fourier modes representation, an isotropic, Gaussian, pseudoturbulence,

$$u_i(\boldsymbol{x}, t) = \sum_{m=1}^{N_k} [b_i^{(m)} \cos(\boldsymbol{k}^{(m)} \cdot \boldsymbol{x} + \omega^{(m)} t) + c_i^{(m)} \sin(\boldsymbol{k}^{(m)} \cdot \boldsymbol{x} + \omega^{(m)} t)] \quad (i = 1, 2, 3), \tag{A 6}$$

is constructed to simulate the fluid turbulence with a specified energy spectrum. In the above, N_k is the number of the random Fourier modes in one flow realization, and $\boldsymbol{k}^{(m)}$ and $\omega^{(m)}$ are the wavenumber and frequency of the mth mode. The random coefficients $b_i^{(m)}$ and $c_i^{(m)}$ are chosen as follows,

$$b_i^{(m)} = \tilde{b}_j^{(m)} (\delta_{ij} - k_i^{(m)} k_j^{(m)} / k^{(m)2}) f(\boldsymbol{k}^{(m)}, \omega^{(m)}), \tag{A 7}$$

where $\tilde{b}_j^{(m)}$ follows a normal distribution with

$$\langle \tilde{b}_j^{(m)} \rangle = 0, \quad \langle \tilde{b}_i^{(m)} \tilde{b}_j^{(m)} \rangle = \delta_{ij}. \tag{A 8}$$

The factor $(\delta_{ij} - k_i^{(m)}k_j^{(m)}/k^{(m)^2})$ in (A 8) ensures the incompressibility $\nabla \cdot \boldsymbol{u} = 0$ for every Fourier mode. The scale factor $f(\boldsymbol{k}, \omega)$ depends on the energy spectrum and the probability density functions (p.d.f.), $p_1(\boldsymbol{k})$ and $p_2(\omega)$, of $\boldsymbol{k}$ and ω,

$$f^2(\boldsymbol{k}, \omega) = \frac{E(k)\tilde{D}(\omega)}{4\pi N k^2 p_1(\boldsymbol{k}) p_2(\omega)}. \tag{A 9}$$

Since $E(k)$ decays as $k^{-5/3}$ in the inertia subrange, a Gaussian distribution for $\boldsymbol{k}$ would lead to a very slow statistical convergence for $u_i(\boldsymbol{x}, t)$. To achieve convergence of the statistics involving the derivatives such as $\partial u_i/\partial x_j$, the following algebraic p.d.f.

$$p_{1i}(k_i) = \tfrac{1}{2}(\mu - 1)(1 + |k_{1i}|)^{-\mu} \quad \text{for} \quad i = 1, 2, 3, \tag{A 10}$$

is used to sample k_i for $k_0 = 1$. The sensitivity of the collision rate α_{ij} to (μ, N_k) is investigated to ensure the statistical convergence at high Re_λ, and independence of the results to these parameters. The frequency $\omega^{(m)}$ is generated with the following p.d.f.

$$p_2(\omega) = \frac{1}{\pi} \frac{1}{1 + (\omega/u_0 k_0)^2}. \tag{A 11}$$

The scale factor is finally set to be

$$f^2(k, \omega) = \frac{E(k)\tilde{D}(w)}{4\pi N_k k^2 p_{11}(k_1) p_{12}(k_2) p_{13}(k_3) p_2(\omega)}. \tag{A 12}$$

It is noted that in the present theoretical formulation, the collision rate is dictated by the spatial structure and the eddy self-decay has no effect on the collision rate. In the numerical simulation of particle collision in isotropic turbulence, the eddy self-decay can be incorporated. Hence, the dependence of $b_i^{(m)}$ and $c_i^{(m)}$ on ω is still included.

A.2. *Rapidly sheared homogeneous turbulence*

For an initially isotropic turbulence under rapid shear, $\Gamma = \partial U/\partial y$, the variation of $b_i^{(m)}$ with time was given in Townsend (1976) based on rapid distortion theory (RDT). Hunt & Carruthers (1990) gave an overview on the use of RDT for representing various types of homogeneous turbulence. Denoting the total shear S as

$$S = \Gamma t \tag{A 13}$$

the new wavenumber vector $\chi^{(m)}$ after the shearing is given by

$$\left.\begin{aligned} \chi_1^{(m)} &= k_1^{(m)}, \\ \chi_2^{(m)} &= k_2^{(m)} - S k_1^{(m)}, \\ \chi_3^{(m)} &= k_3^{(m)}, \end{aligned}\right\} \tag{A 14}$$

where $k^{(m)}$ is the wavenumber vector of the mth mode before the mean shear is applied. The amplitude of each Fourier mode becomes

$$\left.\begin{aligned} b_1^{(m)}(S) &= b_1^{(m)}(0) + a_1 b_2^{(m)}(0), \\ b_2^{(m)}(S) &= a_2 b_2^{(m)}(0), \\ b_3^{(m)}(S) &= b_3^{(m)}(0) + a_3 b_2^{(m)}(0), \end{aligned}\right\} \tag{A 15}$$

where $b_i^{(m)}(0)$ is the corresponding amplitude of the mth mode before the rapid distortion. Dropping the superscript m for convenience, the coefficient a_i for each

mode m is given as

$$\left.\begin{aligned} a_1 = {} & \frac{Sk_1^2}{k_1^2+k_3^2}\frac{k^2-2k_2^2+Sk_1k_2}{\chi^2} - \frac{k^2k_3^2}{(k_1^2+k_3^2)^{3/2}k_1} \\ & \times\left[\tan^{-1}\left(\frac{k}{\sqrt{k_1^2+k_3^2}}\right) - \tan^{-1}\left(\frac{k_2-Sk_1}{\sqrt{k_1^2+k_3^2}}\right)\right], \\ a_2 = {} & k^2/\chi^2, \\ a_3 = {} & \frac{Sk_1k_3}{k_1^2+k_3^2}\frac{k^2-2k_2^2+Sk_1k_2}{\chi^2} - \frac{k^2k_3}{(k_1^2+k_3^2)^{3/2}} \\ & \times\left[\tan^{-1}\left(\frac{k_2}{\sqrt{k_1^2+k_3^2}}\right) - \tan^{-1}\left(\frac{k_2-Sk_1}{\sqrt{k_1^2+k_3^2}}\right)\right], \end{aligned}\right\} \tag{A 16}$$

where $k = \sqrt{k_1^2+k_2^2+k_3^2}$ and $\chi = \sqrt{\chi_1^2+\chi_2^2+\chi_3^2}$. The coefficient $c_i^{(m)}$ is similarly obtained. It is clear from the above that the amplitude of each mode is determined entirely by the total shear $S = \Gamma t$. The dissipation rate $\varepsilon(S)$ can be evaluated as

$$\varepsilon(S)/v = \tfrac{1}{2}\left\langle \sum_{m=1}^{N_k}\left\{\chi^{(m)^2}\sum_{i=1}^{3}[b_i^{(m)^2}(S) + c_i^{(m)^2}(S)]\right\}\right\rangle. \tag{A 17}$$

Finally, the total velocity field is

$$\begin{aligned} u_i(\boldsymbol{x},t) = {} & \sum_{m=1}^{N_k}[b_i^{(m)}(S)\cos(\chi^{(m)}\cdot\boldsymbol{x}+\omega^{(m)}t) + c_i^{(m)}(S)\sin(\chi^{(m)}\cdot\boldsymbol{x}+\omega^{(m)}t)] \\ & +\Gamma x_2\,\delta_{i1} \quad (i=1,2,3). \end{aligned} \tag{A 18}$$

Since the shear rate is high, the term $\omega^{(m)}t$ in the above acts merely as a random phase.

REFERENCES

Balachandar, S. 1988 Particle coagulation in homogeneous turbulence. PhD thesis, Division of Engineering, Brown University, RI.

Chen, M., Kontomaris, K. & Mclaughlin, J. B. 1995 Dispersion, growth, and deposition of coalescing aerosols in a direct numerical simulation of turbulent channel flow. *Gas-Particle Flow*. FED vol. 228, pp. 27–32. ASME.

Hu, K. C. & Mei, R. 1998 A note on particle collision rate in fluid flows. *Phys. Fluids* **10**, 1028–1030.

Hunt, J. C. R. & Carruthers, D. J. 1990 Rapid distortion theory and the 'problems' of turbulence. *J. Fluid Mech.* **212**, 497–532.

Kim, J., Moin, P. & Mosers, R. D. 1987 Turbulence statistics in fully developed channel flow at low Reynolds number. *J. Fluid Mech.* **177**, 133–166.

Kraichnan, R. 1970 Diffusion by a random velocity field. *Phys. Fluids* **13**, 22–31.

Lee, M. J., Kim, J. & Moin, P. 1990 Structure of turbulence at high shear rate. *J. Fluid Mech.* **216**, 561–583.

Mei, R. & Adrian, R. J. 1994 Effect of Reynolds-number-dependent turbulence structure on the dispersion of fluid and particles. *TAM Rep.* 747. Department of Theoretical and Applied Mechanics, University of Illinois, Urbana, Illinois.

Mei, R. & Adrian, R. J. 1995 Effect of Reynolds number on isotropic turbulent dispersion. *Trans. ASME* I: *J. Fluids Engng* **117**, 402–409.

Saffman, P. G. & Turner, J. S. 1956 On the collision of drops in turbulent clouds. *J. Fluid Mech.* **1**, 16–30.

Sato, Y. & Yamamoto, K. 1987 Lagrangian measurement of fluid–particle motion in an isotropic turbulent field. *J. Fluid Mech.* **175**, 183–199.

Smoluchowski, M. V. 1917 Versuch einer mathematischen theorie der koagulationskinetic kolloider losunggen. *Z. Phys. Chem.* **92**, 129.

Sundaram, S. & Collins, L. R. 1997 Collision statistics in an isotropic, particle-laden turbulence suspension. Part 1. Direct numerical simulations. *J. Fluid Mech.* **335**, 75–109.

Townsend, A. A. 1976 *The Structure of Turbulent Shear Flow*, 2nd edn. Cambridge University Press.

Wang, L. P., Wexler, A. S. & Zhou, Y. 1998 On the collision rate of small particles in isotropic turbulence. Part 1. Zero-inertia case. *Phys. Fluids* **10**, 266–276.